Remodeling of the Human Retina in Choroideremia: Rab Escort Protein 1 (*REP-1*) Mutations

Samuel G. Jacobson,[1] *Artur V. Cideciyan,*[1] *Alexander Sumaroka,*[1] *Tomas S. Aleman,*[1] *Sharon B. Schwartz,*[1] *Elizabeth A. M. Windsor,*[1] *Alejandro J. Roman,*[1] *Edwin M. Stone,*[2] *and Ian M. MacDonald*[3]

Purpose. To characterize in detail the disease expression in choroideremia (CHM), a blinding X-linked disease of the retina caused by loss-of-function mutations in Rab Escort Protein 1 (*REP-1*). CHM is readily diagnosed in the clinic and by molecular testing but has lacked an animal model to test hypotheses and therapeutics. The recent report of a mouse model for CHM prompts the need for reassessment of the human disease in anticipation of treatment initiatives.

Methods. CHM hemizygotes with *REP-1* mutations, spanning an age range of 7 decades, were studied with in vivo microscopy by optical coherence tomography.

Results. The disease expression was complex. Earliest stages involved a thickening of the retina that was otherwise normally laminated. Loss of photoreceptors, either independent or associated with retinal pigment epithelium (RPE) depigmentation, was followed by disorganization and further thickening of the retina with interlaminar bridges. The dysmorphic retina then slowly thinned over decades. Laminopathy occurred first in more peripheral rod-rich regions and later in the cone-rich fovea.

Conclusions. The CHM disease sequence involves detectable retinal thickening, which may be due to Müller cell activation and hypertrophy from photoreceptor stress. Photoreceptor degeneration, RPE depigmentation, and retinal remodeling follow. The results represent in vivo evidence in humans for retinal remodeling and provide a marker for the earliest stage of this response to genetic retinal disease. For CHM and other candidate human retinopathies considered for therapy, there is now a framework for making informed decisions about timing, retinal location, and potential value of treatment. (*Invest Ophthalmol Vis Sci.* 2006;47:4113–4120) DOI:10.1167/iovs.06-0424

From the [1]Department of Ophthalmology, Scheie Eye Institute, University of Pennsylvania, Philadelphia, Pennsylvania; [2]Howard Hughes Medical Institute and Department of Ophthalmology, University of Iowa Hospitals and Clinics, Iowa City, Iowa; and the [3]Department of Ophthalmology, University of Alberta, Edmonton, Alberta, Canada.

Supported by the National Institutes of Health, The Foundation Fighting Blindness, the Macula Vision Research Foundation, the F.M. Kirby Foundation, the Macular Disease Foundation, the Ruth and Milton Steinbach Fund, and the Mackall Trust.

Submitted for publication April 13, 2006; revised May 23, 2006; accepted July 25, 2006.

Disclosure: **S.G. Jacobson**, None; **A.V. Cideciyan**, None; **A. Sumaroka**, None; **T.S. Aleman**, None; **S.B. Schwartz**, None; **E.A.M. Windsor**, None; **A.J. Roman**, None; **E.M. Stone**, None; **I.M. MacDonald**, None

The publication costs of this article were defrayed in part by page charge payment. This article must therefore be marked "*advertisement*" in accordance with 18 U.S.C. §1734 solely to indicate this fact.

Corresponding author: Samuel G. Jacobson, Scheie Eye Institute, University of Pennsylvania, 51 N. 39th Street, Philadelphia, PA 19104; jacobsos@mail.med.upenn.edu.

The mature human retina is a central nervous system structure with neurons and glia forming a distinct laminar organization. Mosaics of cells of different type, size, and density fit together to achieve functional neural circuits that transmit visual information to the brain.[1] Among the diseases that disrupt this complex adult retinal structure and lead to blindness are a host of inherited retinal degenerations. Molecular heterogeneity is characteristic of this disease group.[2] A wealth of small and large animal models of the human diseases and increasing preclinical success of somatic gene therapy (for example, Refs. 3–8) have raised expectations that human trials could restore vision in these traditionally incurable forms of genetic blindness.[9–11]

We were prompted to study an inherited human retinal blindness known as choroideremia (CHM) by the recent report that a long-awaited murine model had been genetically engineered.[12] That report signals the start of preclinical and clinical work toward human ocular gene therapy for CHM. Compared with other potentially treatable blinding retinal diseases, human CHM holds the advantages of being clinically easy to detect and molecularly homogeneous. Clinical detection of CHM dates back more than a century; the X-linked genetic pattern has been known for at least 50 years[13,14]; and the molecular basis of disease was discovered approximately 15 years ago.[15] CHM is caused by null mutations in Rab Escort Protein 1 (*REP-1*), a gene involved in the regulation of Rab GTPases and intracellular vesicular transport.[16–18]

As an early step toward translation to human clinical trials in CHM, we explored the disease expression in CHM hemizygotes, spanning an age range of 7 decades. Unexpected and dramatic retinal abnormalities were found by using in vivo high-resolution optical imaging of the otherwise transparent retina in CHM. The disease sequence suggests major remodeling of the human retina. This report represents in vivo evidence for retinal remodeling in humans and emphasizes the need to investigate in detail the human retinal diseases forming the lengthy queue for gene therapy, so that the timing of treatment is appropriate and the potential for efficacy is realistic.

Materials and Methods

Human Subjects

There were 21 CHM hemizygotes representing 15 families. Molecular diagnostics showed that nearly all of these affected males had null alleles in the *CHM* gene (Table 1; Refs. 18,19). Normal subjects (n = 44; ages 5–61 years) were also included. Informed consent was obtained after explanation of the nature of the study; procedures complied with the Declaration of Helsinki and were approved by the institutional review board.

En Face Imaging

A confocal scanning laser ophthalmoscope (Heidelberg Retina Angiogram II, Dossenheim, Germany) was used to image the ocular fundus with infrared (IR) illumination. The contrast of the IR images originates from the interaction of light absorption primarily by RPE pigments and

TABLE 1. Characteristics of Patients with CHM

Patient*	Age at Visit (y)	*CHM* Mutation
P1	6	1168C>T
P2*	7	787C>T
P3	8	EX3_9del
P4	8	1654delG
P5*	11	787C>T
P6†	13	579_587del9ins8
P7	13	787C>T
P8	20	1274 + 1G>A
P9	25	829C>T
P10†	34	579_587del9ins8
P11‡	35	829C>T
P12§	38	146 + 1G>A
P13§	39	146 + 1G>A
P14	40	‖
P15‡	40	829C>T
P16	46	EX9del
P17	49	838C>T
P18	55	787C>T
P19*	56	787C>T
P20	61	838C>T
P21*	61	787C>T

*, †, ‡, § From the same pedigree.
‖ No mutation detected to date.

scattering at the retina, RPE, choroid, and sclera. Localized defects in RPE pigmentation appear as high-intensity regions on these images. Wide-field image montages were assembled from individual images, as previously described.[11,20–22] Optical coherence tomography (OCT) scans were registered to IR image montages by using retinal landmarks.

Optical Coherence Tomography

Cross-sectional retinal reflectivity profiles were obtained with OCT (Carl Zeiss Meditec, Inc., Dublin, CA). The principles of the method and our recording and analysis techniques have been published.[11,20–26] Data were acquired with one of two instruments: OCT1 with a theoretical axial resolution in retinal tissue of ~10 μm or OCT3 with a resolution of ~8 μm. In all subjects, overlapping OCT scans of 4.5 mm length were used to cover horizontal and vertical meridians up to 9 mm eccentricity from the fovea. In a subset of patients, dense raster scans were performed to sample an 18 × 12-mm^2 region of the retina centered on the fovea.[11,20,21] At least three OCTs were obtained at each retinal location. A video fundus image was acquired and saved with each OCT scan by the commercial software. In addition, the fundus video visible during the complete session was recorded continuously on a video cassette recorder.

Postacquisition processing of OCT data was performed with custom programs (MatLab 6.5; The MathWorks, Natick, MA). Longitudinal reflectivity profiles (LRPs) making up the OCT scans were aligned by using a dynamic cross-correlation algorithm[23] with a manual override when crossing structures (for example, RPE depigmentation; see Fig. 1B), which interrupted local lateral isotropy of signals. At extrafoveal retinal regions, two or three repeated scans were averaged to increase signal-to-noise ratio and allow better definition of retinal laminae.[11] At the fovea, a single scan showing the deepest pit was used.

Retinal thickness was defined as the distance between the signal transition at the vitreoretinal interface (labeled T1 in Ref. 23) and major signal peak corresponding to the RPE.[20] In normal subjects, the RPE peak was assumed to be the last peak within the two- or three-peaked scattering signal complex (labeled ORCC in Ref. 23) deep in the retina. In patients, the presumed RPE peak was sometimes the only signal peak deep in the retina; other times, it was apposed by other major peaks (see Figs. 1, 2). In the latter case, the RPE peak was specified manually by considering the properties of the backscattering signal originating from layers vitread and sclerad to it. Outer nuclear layer (ONL) thickness was defined as the major intraretinal signal trough delimited by the signal slope maxima and measured as previously described.[11] In some patients, ONL thickness was not measurable due to laminopathy (see Figs. 1–3).

For topographic analysis, the precise location and orientation of each scan relative to retinal features (blood vessels, RPE depigmentation, and optic nerve head) were determined by using the video images of the fundus. LRPs were allotted to 0.3 × 0.3-mm^2 bins in a rectangular coordinate system centered at the fovea; the waveforms in each bin were aligned and averaged. The retinal thickness was measured as just described, missing data were interpolated bilinearly, thicknesses were mapped to a pseudocolor scale, and the location of blood vessels and optic nerve head was overlaid for reference.[11,21] Lower and upper limits of normal retinal thickness were specified, and the results from patients were subtracted to determine the loci of significant thickening or thinning.

The local extent of RPE depigmentation was estimated by calculating the sub-RPE backscattering index (sRBI), which was defined as the normalized partial integral of the backscattering signal over retinal depth. The partial integral was performed from the RPE signal peak toward the scleral direction until the noise baseline was reached. The partial integral was divided by the signal intensity at the RPE peak to normalize for the pre-RPE attenuation of the light intensity.

Psychophysics

Psychophysical thresholds were measured (1.7° diameter, 200-ms duration stimuli spaced at 2° intervals) in the same retinal regions as the OCT scans. Rod function was determined with two-color, dark-adapted perimetry (500- and 650-nm stimuli). Long/medium-wavelength (L/M) cone function was determined with 650-nm stimuli in the dark-adapted state and compared with normal data determined during the cone plateau phase of dark adaptation after a bleach. Details of the visual function techniques and analysis methods have been published.[11,19–21,26]

RESULTS

Photoreceptor Abnormalities Detected before RPE Depigmentation in CHM Hemizygotes

The clinical diagnosis of CHM is made by en face viewing of the fundus. Unlike the normal homogeneous brown-red background of melanin pigment in RPE and choroid, CHM retinas show patchy depigmentation at early disease stages and progress to extensive pigment loss and visibility of yellow-white sclera through transparent retina. In a conditional knockout of the *Chm* gene (heterozygous-null female mice), retinal morphology suggest that photoreceptor degeneration and patchy depigmentation of the RPE are independent events.[12] Using in vivo cross-sectional optical imaging of the retina in human CHM, we teased apart retinal photoreceptor (PR) from RPE abnormalities, especially focusing on young hemizygotes.

Patchy depigmentation and the immediately adjacent pigmented areas in CHM retinas (Fig. 1A) were sampled by using cross-sectional, high-resolution imaging (Fig. 1B) and compared with images from the same retinal locations in normal subjects (Fig. 1C). The laminar organization inside (transparent part of arrows) and outside (opaque part of arrows) of the depigmented areas is illustrated with overlaid reflectivity profiles. Cross-sections from normal retina show discernible laminae: there are cellular layers of low reflectivity (for example, INL, inner nuclear layer; and ONL) with intervening higher reflectivity laminae of synaptic connections. Deep in the retina is the multipeaked signal representing PR inner and outer segments (IS/OS), RPE, and anterior choroid.[11,20,21] The depigmented patches mainly showed increased backscatter signal, originating from deep to the RPE layer, and disturbed lamination of overlying retina. The deep backscatter corresponded well to the retinal extent of depigmentation from the en face view (see arrows between Figs. 1B, and 1C). The immediately

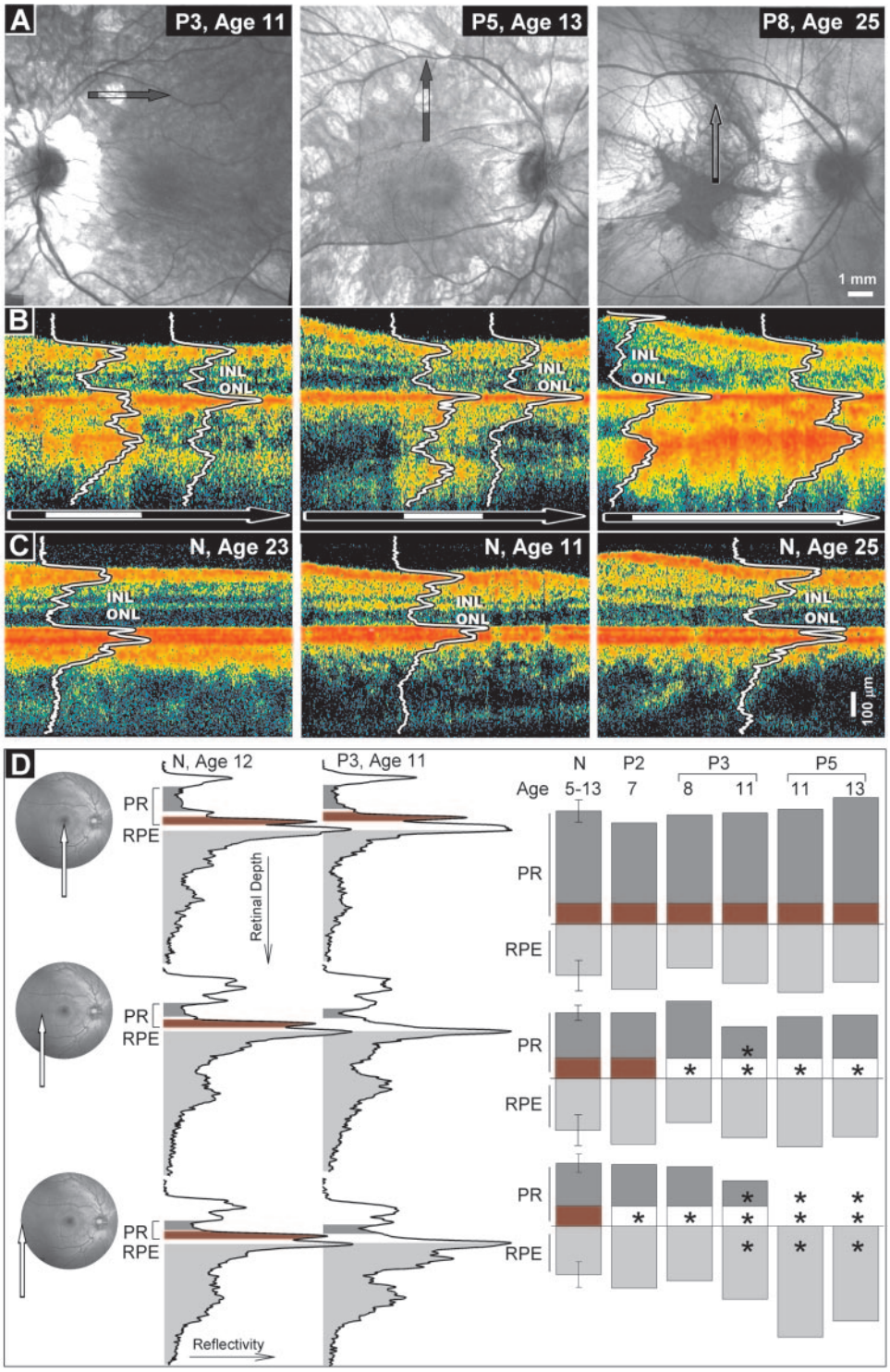

FIGURE 1. Photoreceptor loss precedes RPE depigmentation in human CHM. (**A**) En face images of infrared reflectance in three CHM hemizygote patients show sharp transitions from pigmented to depigmented RPE which were sampled (*arrows*) with cross-sectional scans. (**B**) Cross sections of the regions shown in (**A**). Reflectivity profiles (*white traces*) are overlaid at representative depigmented (*white part of arrows*) and pigmented (*black part of arrows*) retinal locations; signal features representing ONL and INL are shown. (**C**) Cross sections and reflectivity profiles in normal subjects at retinal locations matched to (**B**). (**D**) Quantitation of colocalized photoreceptor (PR) and RPE parameters derived from cross sections at three retinal locations (fovea and 3.6 and 7.8 mm nasal retina; *insets*) in CHM hemizygotes and age-matched normal subjects (N). PR parameters include the thickness of the ONL (*dark gray region*) and existence of the PR-derived signal peak (*red region*). RPE parameter is the normalized backscatter index (*light gray*). PR abnormalities (*) co-occur with normal or abnormal RPE. There are no examples of abnormal RPE with normal PR.

adjacent pigmented areas in the two younger CHM hemizygotes (patient [P]3, P5) retained more normal-appearing laminar architecture and less backscatter. This qualitative approach suggested that the selected areas of depigmentation from en face views also had retinal degeneration.

A quantitative approach was then taken to determine whether photoreceptor degeneration and patchy depigmentation of the RPE were always found together in human CHM (Fig. 1D). Parameters representing photoreceptors (ONL thickness and first peak of multipeaked deep retinal signal[11,20,21]) and RPE depigmentation (sRBI) were measured at three retinal locations (fovea; 3.6 and 7.8 mm in temporal retina) in young CHM hemizygotes (ages 7–13). Representative reflectivity profiles at these different retinal loci show the PR and RPE parameters in a 12-year-old normal subject and P3 at age 11 (Fig. 1D). At the fovea (Fig. 1D, top row), young CHM hemizygotes had photoreceptor and RPE parameters that were within normal limits, calculated from a group of young normal subjects (ages 5–13). At the 3.6-mm temporal retinal locus (Fig. 1D, middle row), all young hemizygotes had normal RPE. P2 at age 7 had normal PR parameters but P3 and P5 (ages 8–13) had loss of the PR IS/OS signal with normal ONL thickness. At 7.8-mm

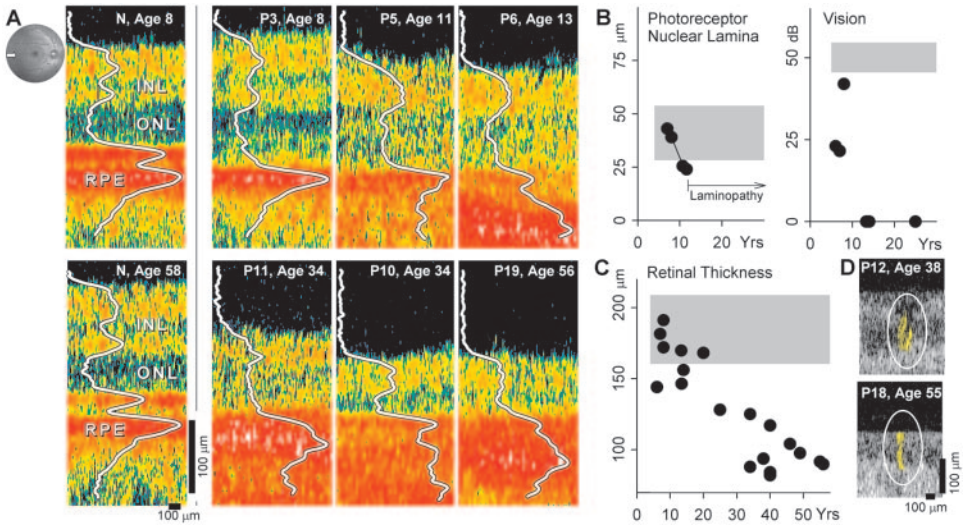

FIGURE 2. Retinal dysmorphology at the rod-rich temporal retina in CHM. (**A**) Cross-sectional scans in representative young (*top row*) and middle aged (*bottom row*) patients and normal (N) subjects. Reflectivity profiles (*white traces*) are overlaid and signal features representing INL, ONL, and RPE are shown. *Inset*: the retinal location sampled. (**B**) Thickness of the ONL in CHM patients (*line connecting symbols* represents P3 at two ages). Laminopathy apparent in patients >11 years of age precludes measurement of ONL thickness. Vision, as defined with dark-adapted absolute sensitivity was abnormal in all patients. (**C**) Overall retinal thickness shows the tendency toward retinal thinning with age. Young patients can show retinas with normal thickness at this location. *Gray regions* in (**B**) and (**C**) represent normal mean ±2 SD (**D**) Representative examples of interlaminar bridges (outlined in *yellow* for visibility) are shown in two CHM patients.

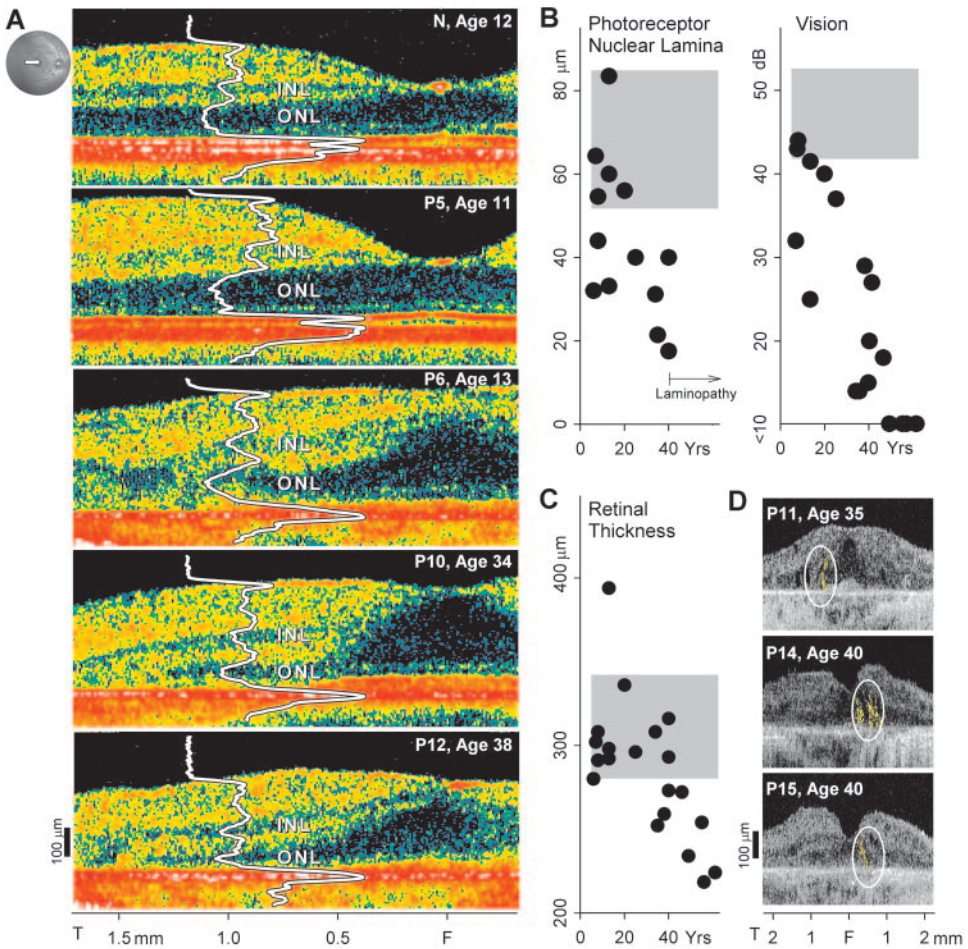

FIGURE 3. Retinal thickening at parafoveal loci in CHM. (**A**) Cross-sectional scans in a normal subject (N) and representative patients along the temporal horizontal meridian crossing the fovea (*inset*: location of scans). Reflectivity profiles (*white traces*) at 1.3-mm eccentricity are shown overlaid on the scans, and signal features corresponding to INL and ONL are marked. (**B**) Photoreceptor (outer) nuclear lamina thickness can range from normal to thin at young ages and is abnormally thinned or undetectable in older patients. Vision at the same parafoveal locus is abnormal in all patients but two. (**C**) Overall retinal thickness as a function of age shows the apparent tendency for thickening at young ages followed by thinning. (**D**) Examples of interlaminar bridges (outlined in *yellow* for visibility) commonly observed in CHM.

eccentricity (Fig. 1D, bottom row), P2 at 7 years and P3 at 8 years had loss of the PR IS/OS signal but normal ONL and RPE parameters. P3 at age 11 and P5 at two ages studied (11 and 13 years) showed evidence for both PR and RPE abnormalities. Therefore, in these young hemizygotes there were detectable micropathological PR abnormalities that colocalized with normal or abnormal RPE, but no evidence was found for RPE abnormality with normal PR.

Photoreceptor Loss and Retinal Dysmorphology with Interlaminar Bridges in Rod-Rich Retina

Retinal lamination is shown for a normal 8-year-old and a normal 58-year-old at a locus 7.8 mm from the fovea in the temporal retina (Fig. 2A, far left panels). Rod photoreceptors in this region are at a density of approximately 120,000 cells/mm^2 and the ratio of rods to cones is ~30:1,[27] resembling the ratio in murine retina.[28] P3 at age 8 years showed a laminar pattern similar to normal with normal ONL thickness but a single rather than multipeaked reflectivity from the outer retina—a feature of PR IS/OS disease.[11,20,21,23] P5 at age 11 retained laminae but the retina was generally thinner, with the ONL more approximate to the RPE, suggesting loss of PR IS/OS; a high backscatter signal was evident deep to the RPE. P6 at age 13 had lost distinct retinal lamination; there was almost a bilaminar appearance with an intense deep backscatter signal. Representative cross-sectional images at ages 34 (P11, P10) and 56 (P19) show disorganized bilaminar retina that is thin in comparison with normal and to scans from the younger CHM hemizygotes.

Only three young CHM hemizygotes (P2 at age 7; P3 at ages 8 and 11; P5, at age 11) had a retinal laminar pattern that permitted measurement of the ONL at this locus. At ≤8 years, the results were within normal limits; but, at age 11, P3 and P5 had reduced ONL thickness (Fig. 2B, left). In other young hemizygotes at ages 11 to 13, the retina had lost laminar organization and ONL measurements were not possible (data not shown). PR-mediated vision at this temporal retinal location indicates minimally or moderately abnormal function at the earliest ages tested and complete loss of sensitivity by about age 13 (Fig. 2B, right). Total retinal thickness at this location presented a data set that contrasted with that of photoreceptor structure and function. There could be normal thickness in many CHM retinas until age 20 years. A slow decline followed over the next 4 decades of life (Fig. 2C). Occasional hyperreflective interlaminar "bridges" were noted between outer and inner retina at this retinal location (Fig. 2D).

Retinal Thickening as a Marker of the Earliest CHM Disease Stage

A more central retinal region extending from 2 mm temporal to the fovea was next evaluated. Cross-sectional images showed a spectrum of changes from normal ONL and normal PR IS/OS, to degenerative stages with PR loss, to retinal laminar disorganization (Fig. 3A). Overlaid reflectivity profiles are at 1.3 mm temporal to the fovea, where rod photoreceptors are at a density of approximately 80,000 cells/mm^2 and the rod-cone ratio is 5:1[20] (Fig. 3A). P5, at age 11, showed normal PR laminae. At the three other ages of CHM hemizygotes shown, there were PR abnormalities: thinning of the ONL and a single rather than multipeaked outer retinal signal indicating IS/OS disturbances. More temporal to the 1.3-mm location, there were hyperreflectivities in the normally hyporeflective zone representing ONL and the appearance of laminar disorganization.

ONL layer thickness was measurable at 1.3 mm temporal retina and declined over the first 4 decades (Fig. 3B); at ages >40 years, the laminar architecture was not distinct enough to be absolutely certain of the ONL. The PR IS/OS signal was lost early in the second decade of life. PR-mediated vision showed

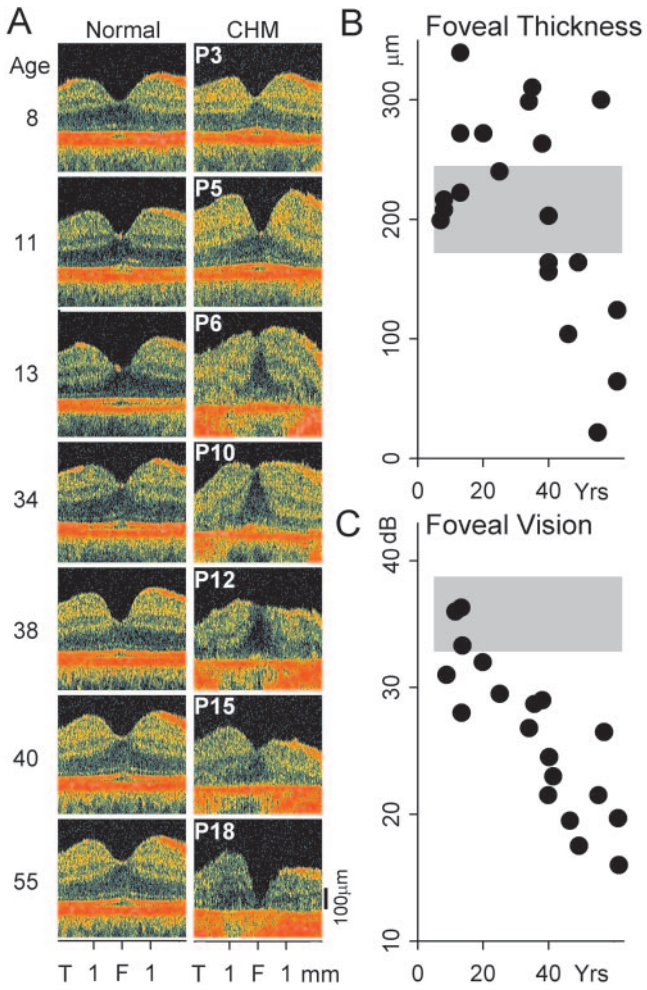

Figure 4. Foveal structure and function in CHM at different ages allow estimation of the natural history of central retinal disease in CHM. (**A**) Cross-sectional scans along the horizontal meridian centered on the fovea. Representative patients are shown age-matched to normal subjects. Scans are vertically aligned by the signal feature corresponding to the RPE. (**B**) Summary of overall retinal thickness measured at the fovea; approximately 30% of all patients show abnormally thickened foveas. (**C**) Summary of foveal vision in all patients shows progressive abnormalities after the first decade of life. *Gray regions:* normal mean ± 2 SD.

a general decline in this region over decades (Fig. 3B). Retinal thickness, in contrast, was either normal or abnormally increased in early years and was maintained within the normal limits until late in the third decade of life; thereafter, there was progressive retinal thinning. A feature captured in many of these cross-sectional images during apparent transition from normal to abnormal lamination were the interlaminar bridges of hyperreflectivity (Fig. 3D).

Cone-Rich Foveal Thickening Decades before Cone Dysfunction

The clinical literature about CHM emphasizes the very long-term preservation of visual acuity.[29] Remarkable changes in foveal architecture, however, were observed in our CHM patients over the lengthy course of disease (Fig. 4). At the earliest ages studied, the CHM fovea had normal architecture, but in patients from ages 13 through 40, there could be extreme thickening of the fovea (Fig. 4A). This obliteration of the normal foveal depression persisted in some subjects, but in others there was eventual thinning (Fig. 4A, age 55).

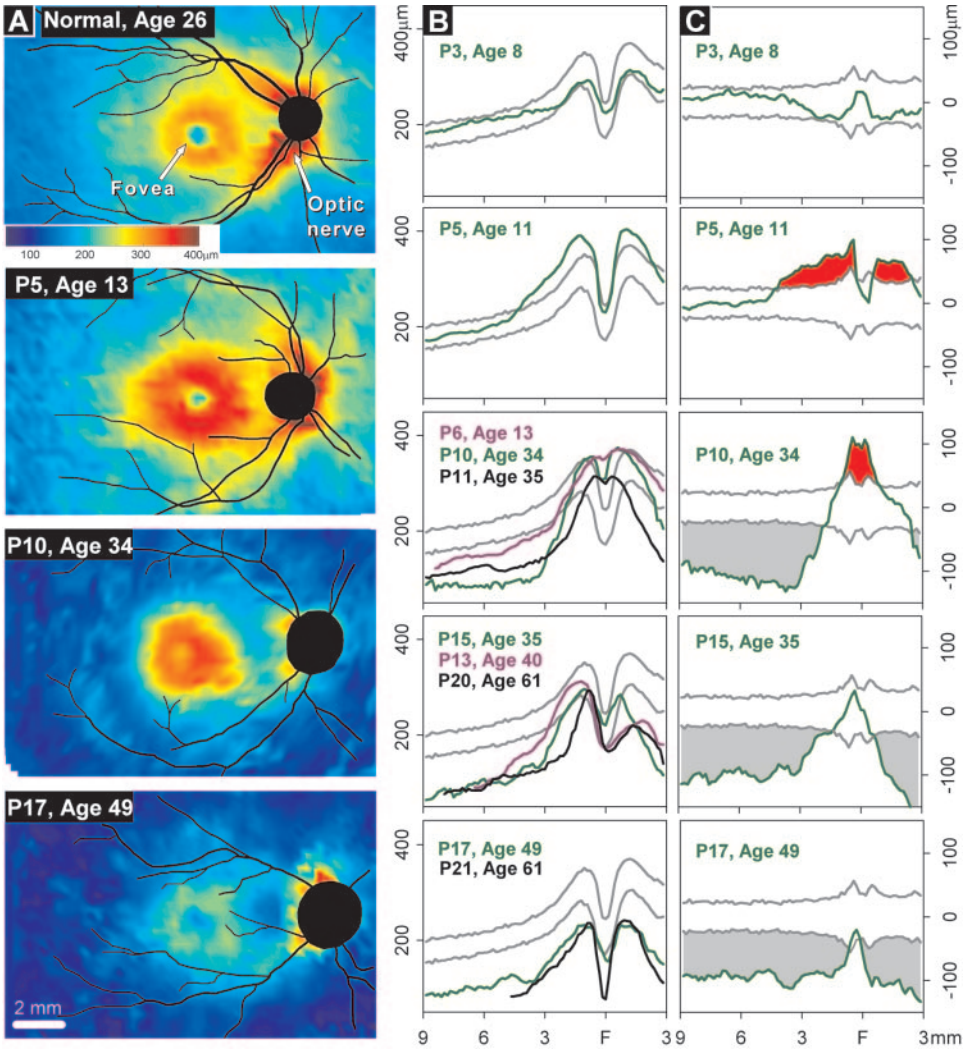

FIGURE 5. Retinal thickness topography of CHM. (**A**) Topographical maps of retinal thickness in a normal subject and CHM hemizygotes representing different ages. All images depicted as right eyes. (**B**) Retinal thickness along the horizontal meridian in representative patients at different ages. (**C**) Difference from mean normal thickness in representative patients to illustrate retinal regions of supernormal (*filled red*) or subnormal (*filled gray*) thickness. *Gray lines* in (**B**) and (**C**): normal mean ± 2 SD.

Foveal thickness was normal in most of the youngest hemizygotes (≤age 13) and then was notably supernormal over ensuing decades (ages 13–38); there was a tendency to decline into the normal range in the fifth decade of life and then become subnormal (Fig. 4B). There was no comparable pattern of foveal cone function increase and then decrease with age. Quantitation of foveal cone sensitivity confirmed the clinical literature of a very slow decline in central function over the decades (Fig. 4C).

Spatiotemporal Pattern of Retinal Thickening

Topographical maps of retinal thickness and measurements across the horizontal meridian (Figs. 5A, 5B) confirmed and extended the sampled data (Figs. 2–4). In the normal human retina, the foveal pit is the site of highest cone density and is surrounded by a parafoveal annulus of increased thickness; there is a gradual decline in retinal thickness with distance from the parafoveal peak to periphery with the exception of the optic nerve head and nerve fiber layers in the nasal retina. In P5, at age 13, the spatial extent of the parafoveal annulus as well as its thickness was abnormally increased. Older hemizygotes could show little or no foveal depression, a normal-appearing parafoveal thickness, and a tendency of thinning with eccentricity. Late stages of the disease, exemplified by P17 at age 49, could show a reappearance of the foveal depression with a very thinned parafovea and periphery (Fig. 5A). A glimpse of the natural history of retinal thickness change was obtained from measurements spanning the horizontal meridian in a group of 10 CHM hemizygotes (Fig. 5B). The differences from mean thickness in representative patients of different ages are illustrated, and the retinal regions with supernormal and subnormal thickness are highlighted; normal limits represent ±2 SD from the mean (Fig. 5C). In the first decade of life, retinal thickness could be normal. Early in the second decade of life, a parafoveal region of abnormally increased thickness became evident. P5 at age 11 illustrates this parafoveal abnormality; there was normal thickness in the more peripheral retina. In the second through fourth decades of life, foveal thickening was frequently observed and there was loss of the foveal pit; the parafovea could be normal in thickness, but there was thinning with increasing eccentricity. P10 at age 34 illustrated the foveal thickening and peripheral thinning. In later decades, there was generalized thinning of central as well as peripheral retina (Figs. 5B, 5C).

DISCUSSION

Neuronal damage in the mature central nervous system elicits complex remodeling responses of neurons and glia.[30–32] Retinal remodeling has been documented in postmortem human donor retinas affected with retinal degeneration[33,34] and in studies of animal retinas in response to genetic and traumatic diseases.[35–38] Interest in retinal remodeling has heightened as

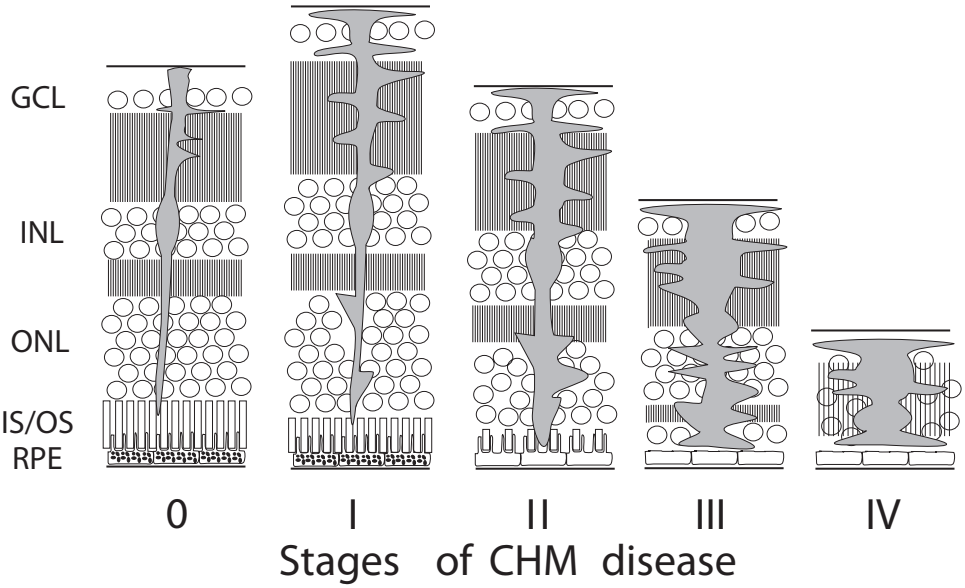

FIGURE 6. Model of human CHM disease sequence. Stage 0 is a schematic of normal retina. Stage I represents the earliest detectable abnormality, consisting of a thickened retina with otherwise normal lamination. Stages II and II represent clinically overt CHM disease with loss of photoreceptor nuclei, shortening of IS/OS, and depigmentation of RPE. The latest disease stage (stage IV) is a thinned retina with neuronal cell death and loss of laminar architecture with gliosis. Müller glial cells: *filled gray*. GCL, ganglion cell layer; INL, inner nuclear layer; ONL, outer nuclear layer; IS/OS, photoreceptor inner and outer segments; RPE, retinal pigment epithelium.

success has increased in treating animal models of human genetic retinal degenerations with gene transfer. The question often posed is how such changes in retinal structure, so well demonstrated in animals, would alter or limit approaches to treatment in humans. A more fundamental and unanswered question is whether retinal remodeling can even be detected in vivo in human retinal degenerations. Until the present study, this question has not been asked.

Our disease analysis of CHM, a candidate retinal blindness for gene therapy, led to the unexpected observation of dramatic alterations in the laminar organization of these retinas. The spectrum and sequence of abnormalities we observed in CHM retinas most likely represent in vivo evidence of remodeling of the human retina in retinal degeneration. The earliest finding was retinal thickening that anticipated or coincided with photoreceptor abnormalities. Of course, there are many possible explanations for retinal thickening. In the context of our entire data set, however, we propose that this thickening is a surrogate marker for the earliest stages of remodeling and that the pathobiology underlying this disease expression involves the Müller cell, the main glial cell of the retina. The radially oriented Müller cells span the retinal depth, contact most neurons, serve a multitude of functions, and are distributed across the primate and human retina including the fovea.[39–43] Activation of glial cells after neuronal injury, whether genetic or traumatic, is a common feature of central nervous system and retinal diseases.[30,32,44] Müller cell activation has even been noted as a presage to photoreceptor loss in aging rats.[45] A signaling pathway between injured photoreceptors and Müller cells has recently been elucidated.[44] We suggest that photoreceptor stress or damage (either primary or secondary to RPE disease) in CHM leads to Müller cell activation, hypertrophy, or possibly proliferation, and this effect is detectable as retinal thickening by in vivo cross-sectional imaging. The tell-tale optical features of radially oriented hyperreflective bridges extending between laminae may represent activated and hypertrophied Müller cell clusters with an altered phenotype that changes the optical properties in cross section. The high density of Müller cells in the parafovea of the primate retina may explain the pronounced thickening near the fovea; in the fovea, Müller cells are the only cell type other than cone photoreceptors.[39,42,46] Other possible contributing sources to retinal thickening could be intracellular edema of neuronal or glial cells, as suggested by studies of neurotrophic factors in retinal degenerations.[47–49]

Beyond these earlier stages, there is photoreceptor dysfunction and death and loss of normal retinal lamination. Taking previous work in animal retinas[35–37] together with our in vivo results, a simplified model involving four major disease stages of CHM can be described (Fig. 6). According to this model, the earliest detectable abnormality is a thickened retina with normal lamination and normal function (stage I). Disease becomes clinically overt with loss of photoreceptor nuclei, shortening of IS/OS, and depigmentation of RPE (stages II and III). The latest disease stage (stage IV) of CHM is a thinned retina with neuronal cell death and loss of laminar architecture, with gliosis. Stage IV retina without discrete laminae in blind regions of CHM retina would probably also show the complex reorganization described in the many histopathological studies of other retinopathies [33–38] Of interest, in human retinopathies caused by mutations in *NR2E3* and *CRB1*, we also observed dysplastic-appearing retina but with topographies different from that in CHM.[20,21] A parsimonious explanation is that retinal remodeling plays a key role in all three disorders; further studies should tell whether most human retinopathies with photoreceptor loss undergo a stereotypical retinal remodeling disease sequence as occurs in many rodent retinopathies.[35,37]

What is the clinical relevance of the current results? An in vivo surrogate marker of the earliest disease stages of retinal remodeling and characterization of later stages should be valuable in the timing of future interventions in CHM as well as in other retinal degenerations that may share these features. For example, late-stage delaminated and thinned retina would obviously not be a candidate region for an intervention intended to restore vision by gene replacement. Regions with retinal thickening but little or no measurable photoreceptor loss may be candidate areas for therapy designed to preserve retina. The latest stage of retinal remodeling at which an intervention would reverse this cascade is unknown but can be tested experimentally in other animal retinal degenerations documented to involve such changes.[35,37] Of interest, the literature on experimental retinal detachment indicates that Müller cell hypertrophy is inhibited by reattachment, but some aspects of Müller cell behavior are not reversed.[50] Recognition that progression to blindness in CHM may result not only from the abnormal REP-1 pathway but also from secondary neuronal death and corrupted retinal circuitry due to irreversible negative effects of remodeling[35,37] should advocate for early intervention in a disease so readily diagnosed clinically and molecularly.

Acknowledgments

The authors thank Andy Cheung, Elaine Smilko, Michelle Doobrajh, Marisa Roman, Kelly McTaggert, Alexandra Windsor, and Malgorzata Swider for critical help.

References

1. Wassle H. Parallel processing in the mammalian retina. *Nat Rev Neurosci*. 2004;5:1–11.
2. Kennan A, Aherne A, Humphries P. Light in retinitis pigmentosa. *Trends Genet*. 2005;21:103–110.
3. Ali RR, Sarra GM, Stephens C, et al. Restoration of photoreceptor ultrastructure and function in retinal degeneration slow mice by gene therapy. *Nat Genet*. 2000;25:306–310.
4. Acland GM, Aguirre GD, Ray J, et al. Gene therapy restores vision in a canine model of childhood blindness. *Nat Genet*. 2001;28:92–95.
5. Vollrath D, Feng W, Duncan JL, et al. Correction of the retinal dystrophy phenotype of the RCS rat by viral gene transfer of Mertk. *Proc Natl Acad Sci USA*. 2001;98:12584–12589.
6. Acland GM, Aguirre GD, Bennett J, et al. Long-term restoration of rod and cone vision by single dose rAAV-mediated gene transfer to the retina in a canine model of childhood blindness. *Mol Ther*. 2005;12:1072–1082.
7. Dinculescu A, Glushakova L, Min SH, Hauswirth WW. Adeno-associated virus-vectored gene therapy for retinal disease. *Hum Gene Ther*. 2005;16:649–663.
8. Batten ML, Imanishi Y, Tu DC, et al. Pharmacological and rAAV gene therapy rescue of visual functions in a blind mouse model of Leber congenital amaurosis. *PloS Med*. 2005;2:e333.
9. Rolling F. Recombinant AAV-mediated gene transfer to the retina: gene therapy perspectives. *Gene Ther*. 2004;11:S26–S32.
10. Preising MN, Heegard S. Recent advances in early-onset severe retinal degeneration: more than just basic research. *Trends Mol Med*. 2004;10:51–54.
11. Jacobson SG, Aleman TS, Cideciyan AV, et al. Identifying photoreceptors in blind eyes caused by RPE65 mutations: prerequisite for human gene therapy success. *Proc Natl Acad Sci USA*. 2005;102:6177–6182.
12. Tolmachova T, Anders R, Abrink M, et al. Independent degeneration of photoreceptors and retinal pigment epithelium in conditional knockout mouse models of choroideremia. *J Clin Invest*. 2006;116:386–394.
13. McCulloch C. Choroideremia: a clinical and pathologic review. *Trans Am Ophthalmol Soc*. 1969;67:142–195.
14. Sorsby A, Franceschetti A, Joseph R, Davey JB. Choroideremia: clinical and genetic aspects. *Br J Ophthalmol*. 1952;36:547–581.
15. Cremers FP, van de Pol DJ, van Kerkhoff LP, Wieringa B, Ropers HH. Cloning of a gene that is rearranged in patients with choroideraemia. *Nature*. 1990;347:674–677.
16. Seabra MC, Mules EH, Hume AN. Rab GTPases, intracellular traffic and disease. *Trends Mol Med*. 2002;8:23–30.
17. Preising M, Ayuso C. Rab escort protein 1 (REP1) in intracellular traffic: a functional and pathophysiological overview. *Ophthalmic Genet*. 2004;25:101–110.
18. MacDonald IM, Sereda C, McTaggert K, Mah D. Choroideremia gene testing. *Expert Rev Mol Diagn*. 2004;4:478–484.
19. Duncan J, Aleman TS, Gardner LM, et al. Macular pigment and lutein supplementation in choroideremia. *Exp Eye Res*. 2002;74:371–381.
20. Jacobson SG, Cideciyan AV, Aleman TS, et al. Crumbs homolog 1 (CRB1) mutations result in a thick human retina with abnormal lamination. *Hum Mol Genet*. 2003;12:1073–1078.
21. Jacobson SG, Sumaroka A, Aleman TS, et al. Nuclear receptor NR2E3 gene mutations distort human retinal laminar architecture and cause an unusual degeneration. *Hum Mol Genet*. 2004;13:1893–1902.
22. Cideciyan AV, Jacobson SG, Aleman TS, et al. In vivo dynamics of retinal injury and repair in the rhodopsin mutant dog model of human retinitis pigmentosa. *Proc Natl Acad Sci USA*. 2005;102:5233–5238.
23. Huang Y, Cideciyan AV, Papastergiou GI, et al. Relation of optical coherence tomography to microanatomy in normal and rd chickens. *Invest Ophthalmol Vis Sci*. 1998;39:2405–2416.
24. Huang D, Swanson EA, Lin CP, et al. Optical coherence tomography. *Science*. 1991;254:1178–1181.
25. Drexler W, Morgner U, Ghanta RK, Kartner FX, Schuman JS, Fujimoto JG. Ultrahigh-resolution ophthalmic optical coherence tomography. *Nat Med*. 2001;7:502–507.
26. Jacobson SG, Cideciyan AV, Iannaccone A, et al. Disease expression of RP1 mutations causing autosomal dominant retinitis pigmentosa. *Invest Ophthalmol Vis Sci*. 2000;41:1898–1908.
27. Curcio CA, Sloan KR, Kalina RE, Hendrickson AE. Human photoreceptor topography. *J Comp Neurol*. 1990;292:497–523.
28. Carter-Dawson LD, LaVail MM. Rods and cones in the mouse retina. I. Structural analysis using light and electron microscopy. *J Comp Neurol*. 1979;188:245–262.
29. Roberts MF, Fishman GA, Roberts DK, et al. Retrospective, longitudinal, and cross sectional study of visual acuity impairment in choroideraemia. *Br J Ophthalmol*. 2002;86:658–662.
30. Chen S, Pickard JD, Harris NG. Time course of cellular pathology after controlled cortical impact injury. *Exp Neurol*. 2003;182:87–102.
31. Sutula T. Mechanisms of epilepsy progression: current theories and perspectives from neuroplasticity in adulthood and development. *Epilepsy Res*. 2004;60:161–171.
32. Gaudreault SB, Blain JF, Gratton JP, Poirier J. A role for caveolin-1 in post-injury reactive neuronal plasticity. *J Neurochem*. 2005;92:831–839.
33. Milam AH, Li ZY, Fariss RN. Histopathology of the human retina in retinitis pigmentosa. *Prog Retin Eye Res*. 1998;17:175–205.
34. Li ZY, Kljavin IJ, Milam AH. Rod photoreceptor neurite sprouting in retinitis pigmentosa. *J Neurosci*. 1995;15:5429–5438.
35. Marc RE, Jones BW, Watt CB, Strettoi E. Neural remodeling in retinal degeneration. *Prog Retin Eye Res*. 2003;22:607–655.
36. Fisher SK, Lewis GP, Linberg KA, Verardo MR. Cellular remodeling in mammalian retina: results from studies of experimental retinal detachment. *Prog Retin Eye Res*. 2005;24:395–431.
37. Jones BW, Marc RE. Retinal remodeling during retinal degeneration. *Exp Eye Res*. 2005;81:123–137.
38. Wang S, Lu B, Lund RD. Morphological changes in the Royal College of Surgeons rat retina during photoreceptor degeneration and after cell-based therapy. *J Comp Neurol*. 2005;491:400–417.
39. Distler C, Dreher Z. Glia cells of the monkey retina: II. Muller cells. *Vision Res*. 1996;36:2381–2394.
40. Nishikawa S, Tamai M. Muller cells in the human foveal region. *Curr Eye Res*. 2001;22:34–41.
41. Bringmann A, Reichenbach A. Role of Muller cells in retinal degenerations. *Front Biosci.* 2001;6:E72–E92.
42. Burris C, Klug K, Ngo IT, Sterling P, Schein S. How Muller glial cells in macaque fovea coat and isolate the synaptic terminals of cone photoreceptors. *J Comp Neurol*. 2002;453:100–111.
43. Guidry C. The role of Muller cells in fibrocontractive retinal disorders. *Prog Retin Eye Res*. 2005;24:75–86.
44. Rattner A, Nathans J. The genomic response to retinal disease and injury: evidence for endothelin signaling from photoreceptors to glia. *J Neurosci*. 2005;25:4540–4549.
45. DiLoreto DA Jr, Martzen MR, del Cerro C, Coleman PD, del Cerro M. Muller cell changes precede photoreceptor cell degeneration in the age-related retinal degeneration of the Fischer 344 rat. *Brain Res*. 1995;698:1–14.
46. Gass JD. Muller cell cone, an overlooked part of the anatomy of the fovea centralis: hypotheses concerning its role in the pathogenesis of macular hole and foveomacular retinoschisis. *Arch Ophthalmol*. 1999;117:821–823.
47. Bok D, Yasumura D, Matthes MT, et al. Effects of adeno-associated virus-vectored ciliary neurotrophic factor on retinal structure and function in mice with a P216L rds/peripherin mutation. *Exp Eye Res.* 2002;74:719–735.
48. Bush RA, Lei B, Tao W, et al. Encapsulated cell-based intraocular delivery of ciliary neurotrophic factor in normal rabbit: dose-dependent effects on ERG and retinal histology. *Invest Ophthalmol Vis Sci.* 2004;45:2420–2430.
49. Zeiss CJ, Allore HG, Towle V, Tao W. CNTF induces dose-dependent alterations in retinal morphology in normal and rcd-1 canine retina. *Exp Eye Res*. 2006;82:395–404.
50. Fisher SK, Lewis GP. Muller cell and neuronal remodeling in retinal detachment and reattachment and their potential consequences for visual recovery: a review and reconsideration of recent data. *Vision Res*. 2003;43:887–897.